Supplementary Information

Kinetic, thermodynamic, and *ab initio* insights of AsnGly isomerisation as a ticking time bomb for protein integrity

Fruzsina Pilhál[a],[b], Imre Jákli[a],[c], Ernő Keszei[d], András Láng[a] and András Perczel*[a],[c]

[a] F. Pilhál, Dr. I. Jákli, Dr. A. Láng, Prof. A. Perczel
Laboratory of Structural Chemistry and Biology, Institute of Chemistry
ELTE Eötvös Loránd University
Pázmány Péter sétány 1/A, 1117, Budapest, Hungary
E-mail: A.P. perczel.andras@ttk.elte.hu

[b] F. Pilhál
Hevesy György PhD School of Chemistry
ELTE Eötvös Loránd University
Pázmány Péter sétány 1/A, 1117, Budapest, Hungary

[c] Dr. I. Jákli, Prof. A. Perczel
HUN-REN–ELTE Protein Modelling Research Group
ELTE Eötvös Loránd University
Pázmány Péter sétány 1/A, 1117, Budapest, Hungary
E-mail: A.P. perczel.andras@ttk.elte.hu

[d] Prof. E. Keszei
Department of Physical Chemistry and Chemical Kinetics Laboratory, Institute of Chemistry
ELTE Eötvös Loránd University
Pázmány Péter sétány 1/A, 1117, Budapest, Hungary

Table of Contents

Supplementary Note 1 ^{1}H-NMR spectra recording, processing, and analysis procedures

Most of the 1D ^{1}H-NMR spectra (Supplementary Figure 1) with zgesgp pulse program were measured with the following parameters: TD (time domain) = 32768, NS (number of scans) = 64 or 128 or 254, SW (spectral width) = 14.0 ppm, AQ (acquisition time) = 1.7 sec, d1 (delay time) = 0.4 sec, LB (line broadening of exponential window function) = 0.3 Hz.

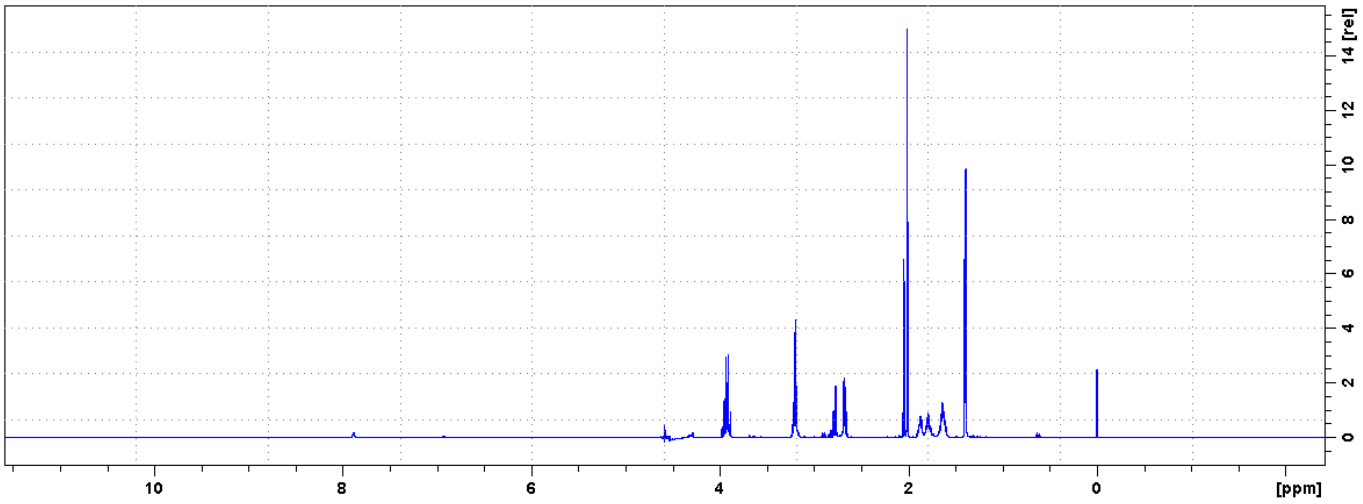

Supplementary Figure 1 **An 1D ^{1}H-NMR spectrum of Ac-NGRA-NH$_2$ measured at pH=7.4 and 46 °C.**

In all spectra the processing started with the *efp* command, then the 0th order correction was done manually for each spectra. After phasing, the DSS signal was calibrated to 0 ppm. By overlaying the spectra calibrated to 0 ppm, the integration limits (regions) for the peptide signals were also determined. The integration limits were determined manually for each measurement condition separately, and the resulting relative integral values and chemical shift values were collected. Then spectra with insufficient shimming or baseline errors were removed from the collected measurement data. The parameter estimation for the remaining data points were then performed using the Copasi software. The exact background for the setup of the kinetic model is discussed in the Kinetic inference of NMR data subsection in the manuscript.

Supplementary Note 2 Detailed kinetic analysis

A. Kinetic inference of NMR data

As the precision of the estimated rate coefficients k_{-2} and k_{-3} for the reverse reactions was not sufficient to obtain reasonable temperature dependence and activation energies based on the Arrhenius equation, we took advantage of the fact that both reversible reactions were first order in both directions. In such cases, $K_2 = \frac{k_2}{k_{-2}}$ and, $K_3 = \frac{k_3}{k_{-3}}$, and based on the Transition State Theory expression of the rate coefficient $k = \frac{k_B T}{h} e^{\frac{-\Delta G^{\ddagger}}{RT}}$ we can write the following:

$$\frac{k_2}{k_{-2}} = K_2 = e^{\frac{\Delta G^{\ddagger}_{-2} - \Delta G^{\ddagger}_{2}}{RT}}, \qquad \text{Supplementary Equation (1)}$$

$$\frac{k_3}{k_{-3}} = K_3 = e^{\frac{\Delta G^{\ddagger}_{-3} - \Delta G^{\ddagger}_{3}}{RT}}. \qquad \text{Supplementary Equation (2)}$$

From these relations we can get the difference of the two activation energies as

$$\Delta G^{\ddagger}_{-2} - \Delta G^{\ddagger}_{2} = RTlnK_2 \text{ and } \Delta G^{\ddagger}_{-3} - \Delta G^{\ddagger}_{3} = RTlnK_3. \qquad \text{Supplementary Equation (3)}$$

Thus, in principle, we could calculate the difference in activation Gibbs free energies from the equilibrium constant determined at a single temperature. Our procedure was to use equilibrium constants at all temperatures where we had a well-determined equilibrium constant, and to use the average of the values thus obtained - assuming temperature independence of reaction enthalpy and entropy in the actual temperature range - to calculate activation energies for the reverse reactions by adding this difference to the activation energy estimated for the forward reactions, again taking into account error propagation. We thus obtained robust estimates of these parameters, automatically matching the values of K_2 and K_3, both greater than 1.

In the temperature range of 28-55 ºC, the pre-exponential coefficient of the Arrhenius equation used to determine the activation energy can be considered temperature independent, but it carries structural information due to the partition functions in the second term. This follows from the above equation derived from Transition State Theory:

$$k = \frac{k_B T}{h} \frac{N_A q^{\ominus}_{\ddagger}}{q^{\ominus}_{AB} q^{\ominus}_{C}} e^{-\frac{E_0}{RT}}. \qquad \text{Supplementary Equation (4)}$$

This means that if a peptide can adopt a structure other than the disordered one, its activation energy cannot be calculated without determining the pre-exponential coefficient.

Supplementary Table 1 The change of Gibbs free energies $\Delta G^{\ddagger}$ (kJ mol^{-1}) of the Suc ($\Delta G^{\ddagger}(1)$, $\Delta G^{\ddagger}(-2)$, $\Delta G^{\ddagger}(-3)$), β-Asp ($\Delta G^{\ddagger}(2)$) and α-Asp ($\Delta G^{\ddagger}(3)$) formation steps for different model peptides.

peptide		$\Delta G^{\ddagger}(1)$	$\Delta G^{\ddagger}(2)$	$\Delta G^{\ddagger}(-2)$	$\Delta G^{\ddagger}(3)$	$\Delta G^{\ddagger}(-3)$
-NGAA-	estimated value [a]	110.8	107.1	118.2	73.5	84.6
	error [a]	0.9	1.5	3.0	6.0	13.5
-NGEA-	estimated value	94.7	61.2	119.4	56.0	n. d. [b]
	error	3.4	23.8	16.5	22.4	40.1
-NGKA-	estimated value	87.3	85.9	89.0	n. d.	n. d.
	error	1.6	2.2	51.6	n. d.	n. d.
-NGRA-	estimated value	97.3	108.0	n. d.	97.3	n. d.
	error	n. d.	n. d.	n. d.	n. d.	n. d.

[a] The term ‘estimated value’ refers to the parameter estimation result based on the fit of mechanism (1) to the temporal evolution of all four species, while 'error' refers to the half-widths of their 95% confidence intervals.

[b] Symbol ‘n. d.’ stands for ‘not determined’; in these cases, a significant value of activation energies could not be inferred, due to large uncertainties in the time-dependent concentrations of the modified peptides.

B. Diagrams of the measured and fitted relative concentrations determined by the parameter estimation process.

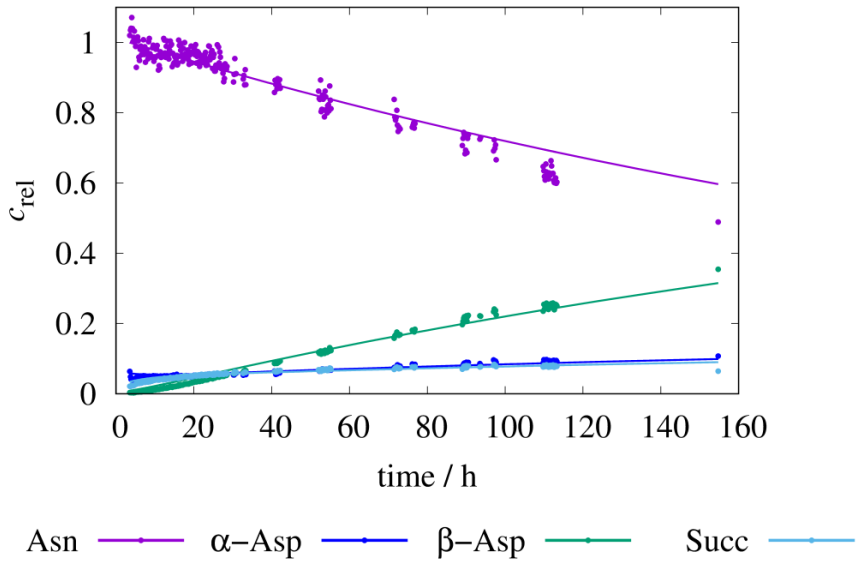

Supplementary Figure 2 **The measured and fitted time course of the Ac-NGAA-NH_2 isomerisation reaction at pH=5.1, 55 °C.** The decomposition of Ac-NGAA-NH_2 via isomerisation and the formation of the products β-Asp (β-DGAA) and α-Asp (α-DGAA), respectively (pH=5.1, T=55 °C), via the intermediate succinimide (Suc). The vertical axis is scaled with arbitrary units proportional to selected non-overlapping NMR signal integrals plotted as a function of the time.

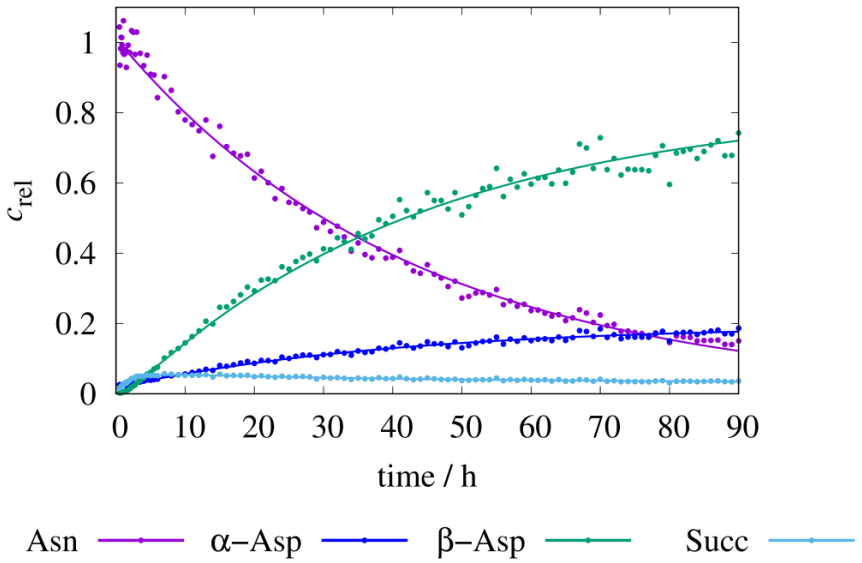

Supplementary Figure 3 **The measured and fitted time course of the Ac-NGAA-NH_2 isomerisation reaction at pH=6.3, 55 °C.** The decomposition of Ac-NGAA-NH_2 via isomerisation and the formation of the products β-Asp (β-DGAA) and α-Asp (α-DGAA), respectively (pH=6.3, T=55 °C), via the intermediate succinimide (Suc). The vertical axis is scaled with arbitrary units proportional to selected non-overlapping NMR signal integrals plotted as a function of the time.

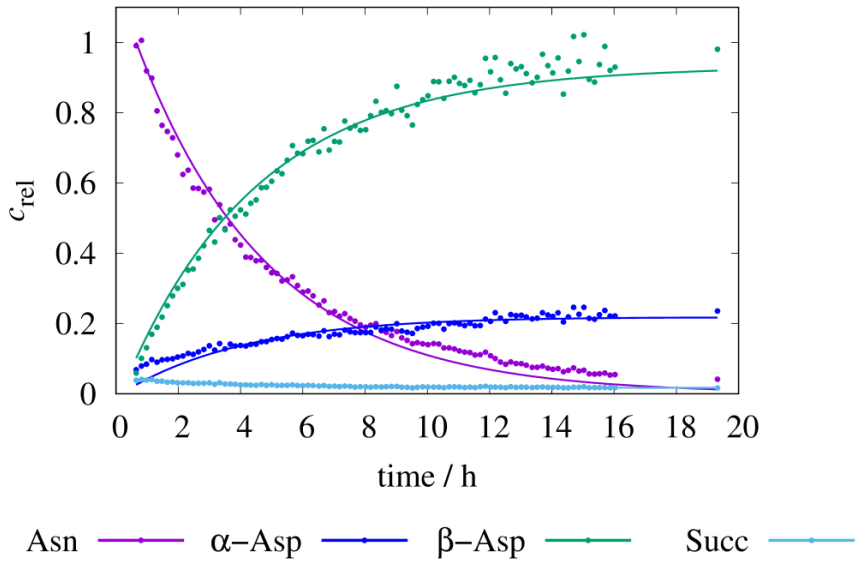

Supplementary Figure 4 **The measured and fitted time course of the Ac-NGAA-NH_2 isomerisation reaction at pH=7.4, 55 °C.** The decomposition of Ac-NGAA-NH_2 via isomerisation and the formation of the products β-Asp (β-DGAA) and α-Asp (α-DGAA), respectively (pH=7.4, T=55 °C), via the intermediate succinimide (Suc). The vertical axis is scaled with arbitrary units proportional to selected non-overlapping NMR signal integrals plotted as a function of the time.

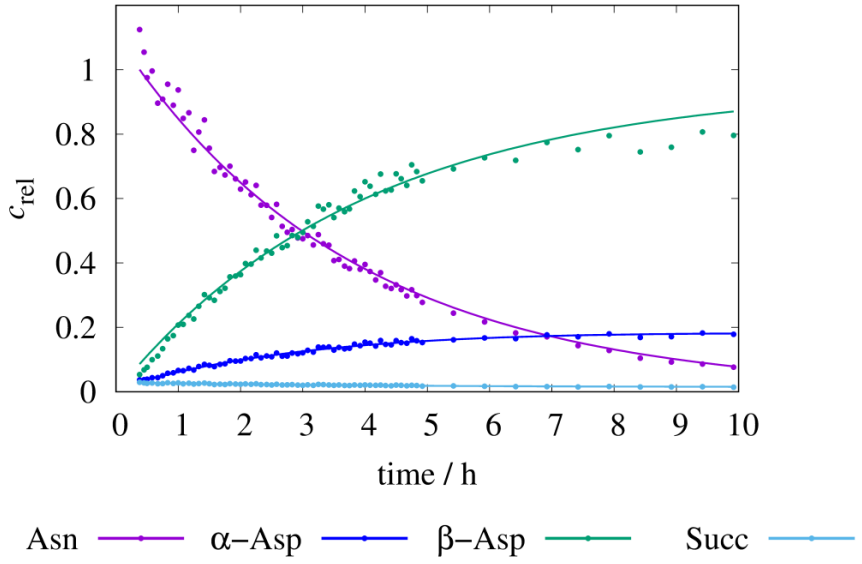

Supplementary Figure 5 **The measured and fitted time course of the Ac-NGAA-NH_2 isomerisation reaction at pH=7.8, 55 °C.** The decomposition of Ac-NGAA-NH_2 via isomerisation and the formation of the products β-Asp (β-DGAA) and α-Asp (α-DGAA), respectively (pH=7.8, T=55 °C), via the intermediate succinimide (Suc). The vertical axis is scaled with arbitrary units proportional to selected non-overlapping NMR signal integrals plotted as a function of the time.

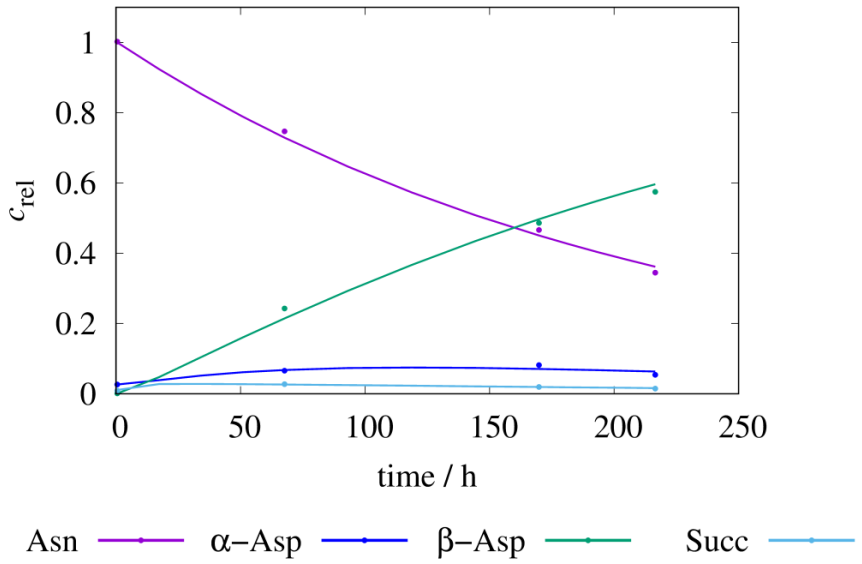

Supplementary Figure 6 **The measured and fitted time course of the Ac-NGAA-NH_2 isomerisation reaction at pH=7.4, 28 °C.** The decomposition of Ac-NGAA-NH_2 via isomerisation and the formation of the products β-Asp (β-DGAA) and α-Asp (α-DGAA), respectively (pH=7.4, T=28 °C), via the intermediate succinimide (Suc). The vertical axis is scaled with arbitrary units proportional to selected non-overlapping NMR signal integrals plotted as a function of the time.

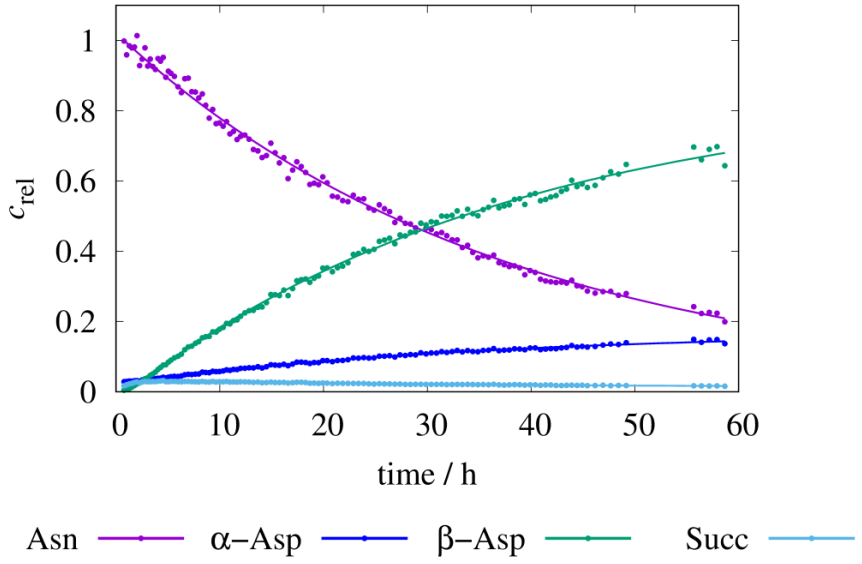

Supplementary Figure 7 **The measured and fitted time course of the Ac-NGAA-NH_2 isomerisation reaction at pH=7.4, 37 °C.** The decomposition of Ac-NGAA-NH_2 via isomerisation and the formation of the products β-Asp (β-DGAA) and α-Asp (α-DGAA), respectively (pH=7.4, T=37 °C), via the intermediate succinimide (Suc). The vertical axis is scaled with arbitrary units proportional to selected non-overlapping NMR signal integrals plotted as a function of the time.

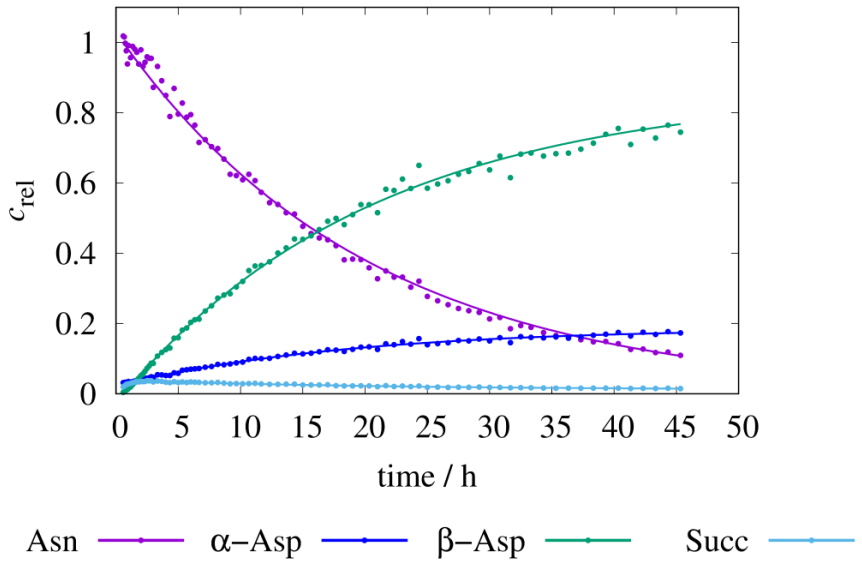

Supplementary Figure 8 **The measured and fitted time course of the Ac-NGAA-NH_2 isomerisation reaction at pH=7.4, 46 °C.** The decomposition of Ac-NGAA-NH_2 via isomerisation and the formation of the products β-Asp (β-DGAA) and α-Asp (α-DGAA), respectively (pH=7.4, T=46 °C), via the intermediate succinimide (Suc). The vertical axis is scaled with arbitrary units proportional to selected non-overlapping NMR signal integrals plotted as a function of the time.

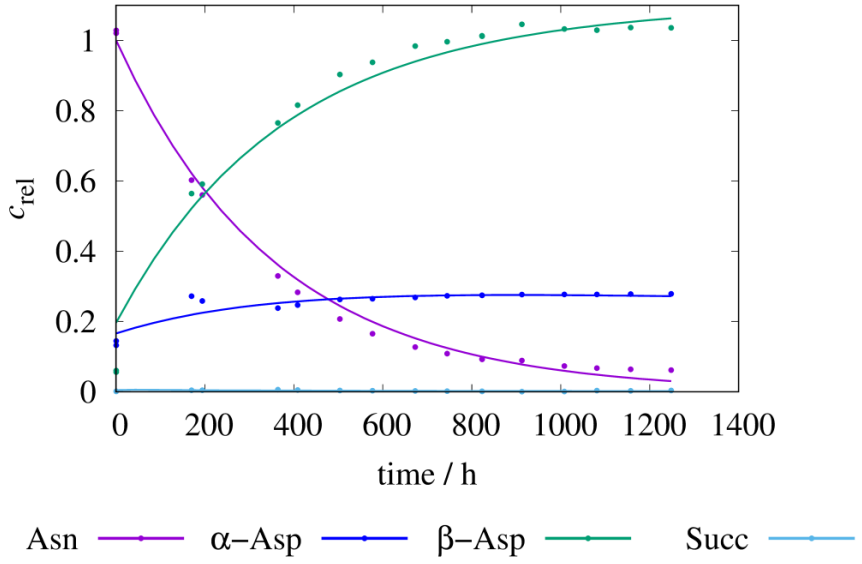

Supplementary Figure 9 **The measured and fitted time course of the Ac-NGEA-NH_2 isomerisation reaction at pH=7.4, 28 °C.** The decomposition of Ac-NGEA-NH_2 via isomerisation and the formation of the products β-Asp (β-DGAA) and α-Asp (α-DGAA), respectively (pH=7.4, T=28 °C), via the intermediate succinimide (Suc). The vertical axis is scaled with arbitrary units proportional to selected non-overlapping NMR signal integrals plotted as a function of the time.

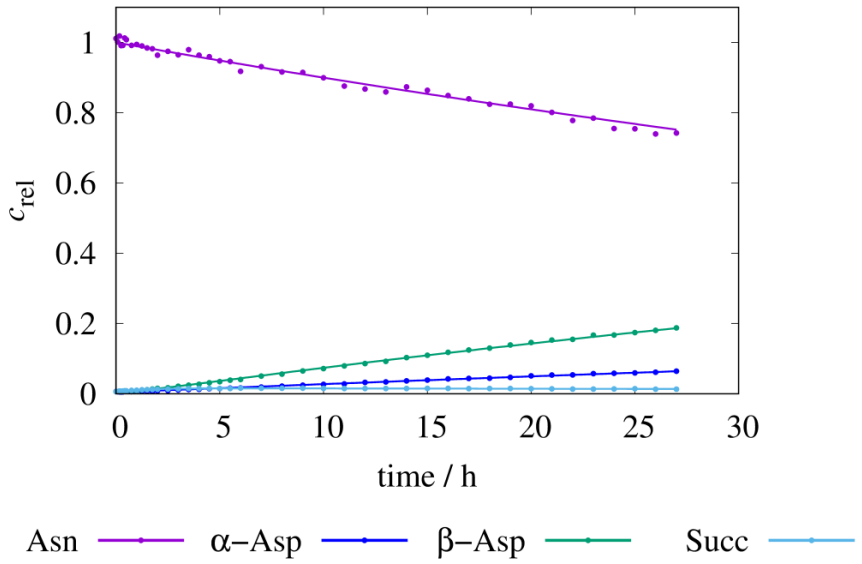

Supplementary Figure 10 **The measured and fitted time course of the Ac-NGEA-NH_2 isomerisation reaction at pH=7.4, 37 °C.** The decomposition of Ac-NGEA-NH_2 via isomerisation and the formation of the products β-Asp (β-DGAA) and α-Asp (α-DGAA), respectively (pH=7.4, T=37 °C), via the intermediate succinimide (Suc). The vertical axis is scaled with arbitrary units proportional to selected non-overlapping NMR signal integrals plotted as a function of the time.

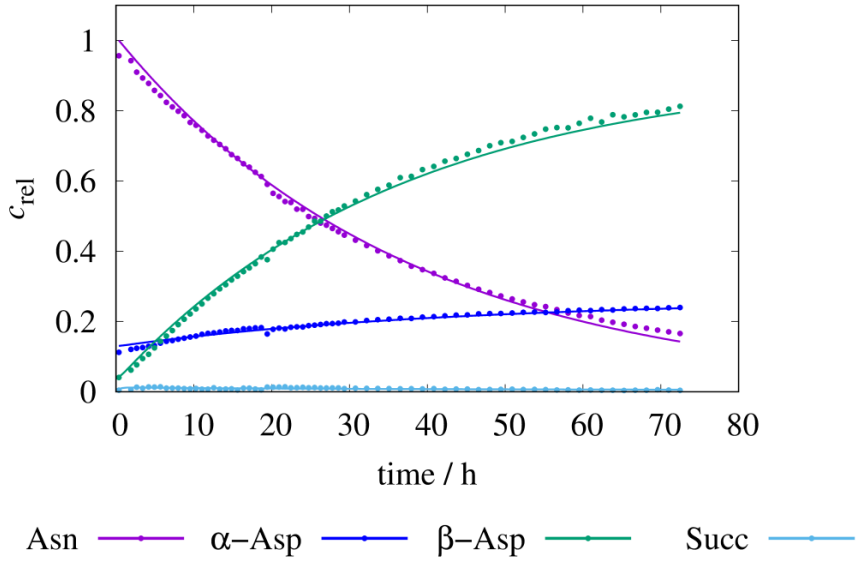

Supplementary Figure 11 **The measured and fitted time course of the Ac-NGEA-NH_2 isomerisation reaction at pH=7.4, 46 °C.** The decomposition of Ac-NGEA-NH_2 via isomerisation and the formation of the products β-Asp (β-DGAA) and α-Asp (α-DGAA), respectively (pH=7.4, T=46 °C), via the intermediate succinimide (Suc). The vertical axis is scaled with arbitrary units proportional to selected non-overlapping NMR signal integrals plotted as a function of the time.

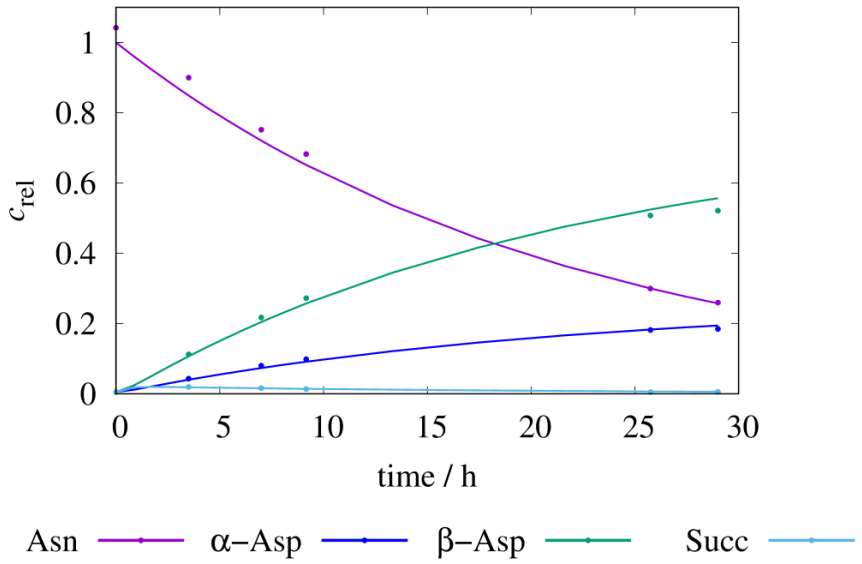

Supplementary Figure 12 **The measured and fitted time course of the Ac-NGEA-NH_2 isomerisation reaction at pH=7.4, 55 °C.** The decomposition of Ac-NGEA-NH_2 via isomerisation and the formation of the products β-Asp (β-DGAA) and α-Asp (α-DGAA), respectively (pH=7.4, T=55 °C), via the intermediate succinimide (Suc). The vertical axis is scaled with arbitrary units proportional to selected non-overlapping NMR signal integrals plotted as a function of the time.

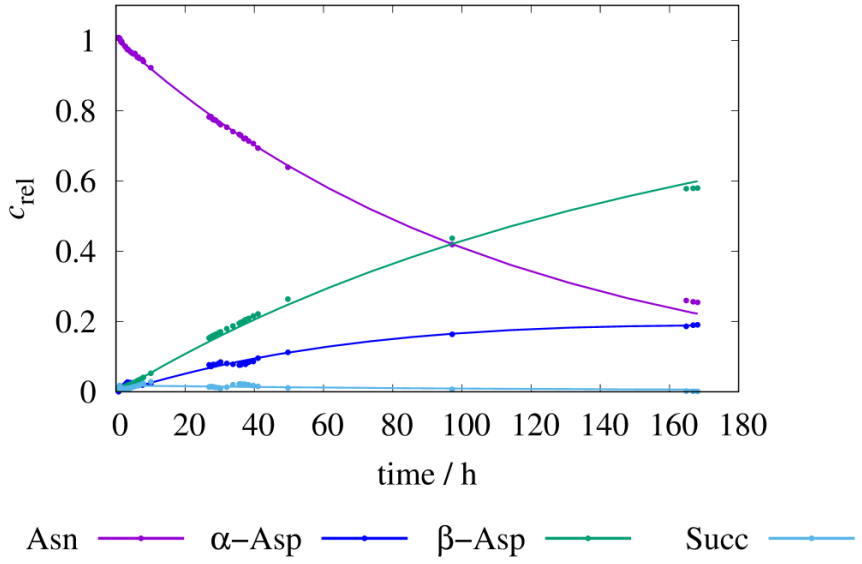

Supplementary Figure 13 **The measured and fitted time course of the Ac-NGKA-NH_2 isomerisation reaction at pH=7.4, 28 °C.** The decomposition of Ac-NGKA-NH_2 via isomerisation and the formation of the products β-Asp (β-DGAA) and α-Asp (α-DGAA), respectively (pH=7.4, T=28 °C), via the intermediate succinimide (Suc). The vertical axis is scaled with arbitrary units proportional to selected non-overlapping NMR signal integrals plotted as a function of the time.

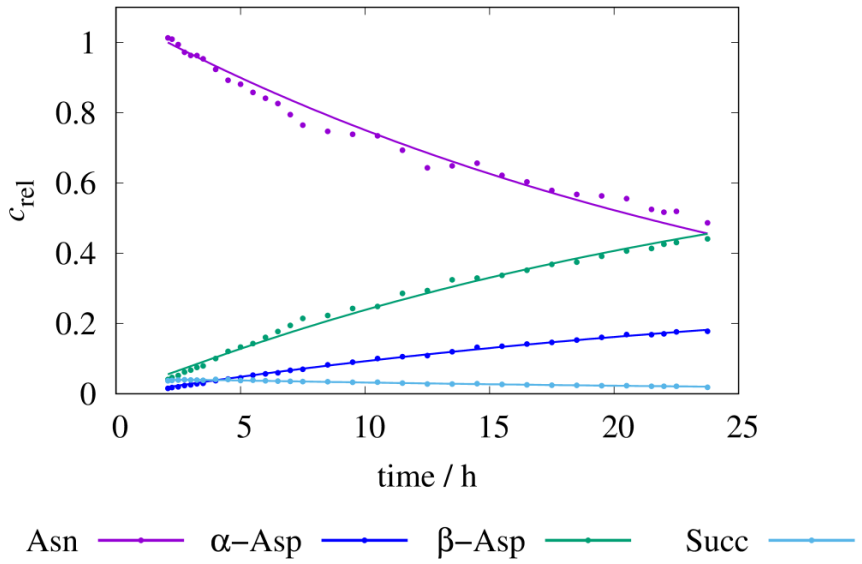

Supplementary Figure 14 **The measured and fitted time course of the Ac-NGKA-NH_2 isomerisation reaction at pH=7.4, 37 °C.** The decomposition of Ac-NGKA-NH_2 via isomerisation and the formation of the products β-Asp (β-DGAA) and α-Asp (α-DGAA), respectively (pH=7.4, T=37 °C), via the intermediate succinimide (Suc). The vertical axis is scaled with arbitrary units proportional to selected non-overlapping NMR signal integrals plotted as a function of the time.

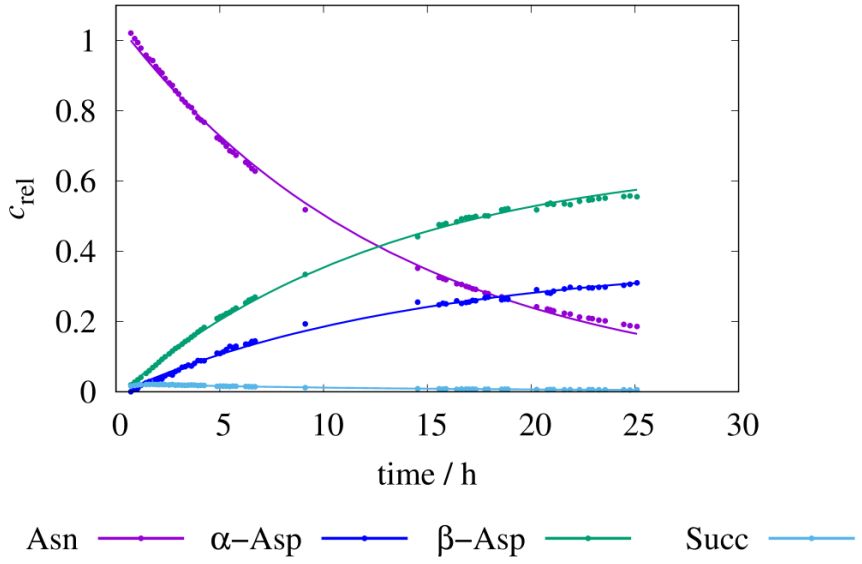

Supplementary Figure 15 **The measured and fitted time course of the Ac-NGKA-NH_2 isomerisation reaction at pH=7.4, 46 °C.** The decomposition of Ac-NGKA-NH_2 via isomerisation and the formation of the products β-Asp (β-DGAA) and α-Asp (α-DGAA), respectively (pH=7.4, T=46 °C), via the intermediate succinimide (Suc). The vertical axis is scaled with arbitrary units proportional to selected non-overlapping NMR signal integrals plotted as a function of the time.

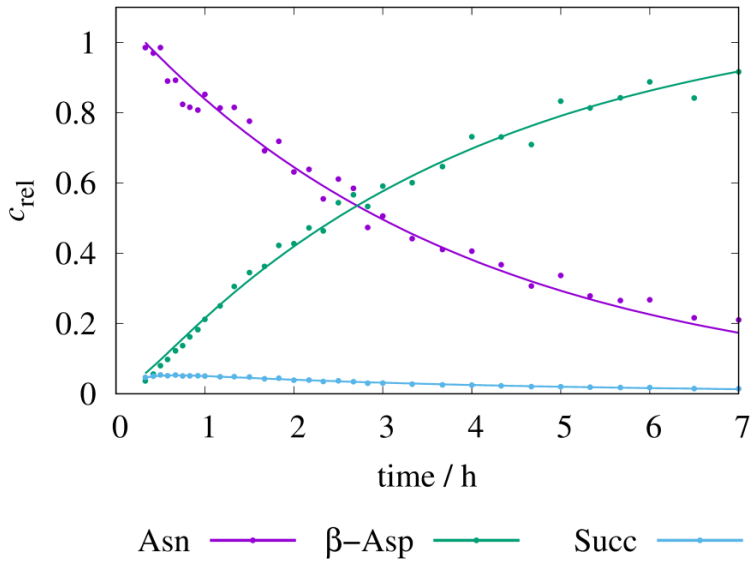

Supplementary Figure 16 **The measured and fitted time course of the Ac-NGKA-NH_2 isomerisation reaction at pH=7.4, 55 °C.** The decomposition of Ac-NGKA-NH_2 via isomerisation and the formation of the products β-Asp (β-DGAA) and α-Asp (α-DGAA), respectively (pH=7.4, T=55 °C), via the intermediate succinimide (Suc). The vertical axis is scaled with arbitrary units proportional to selected non-overlapping NMR signal integrals plotted as a function of the time.

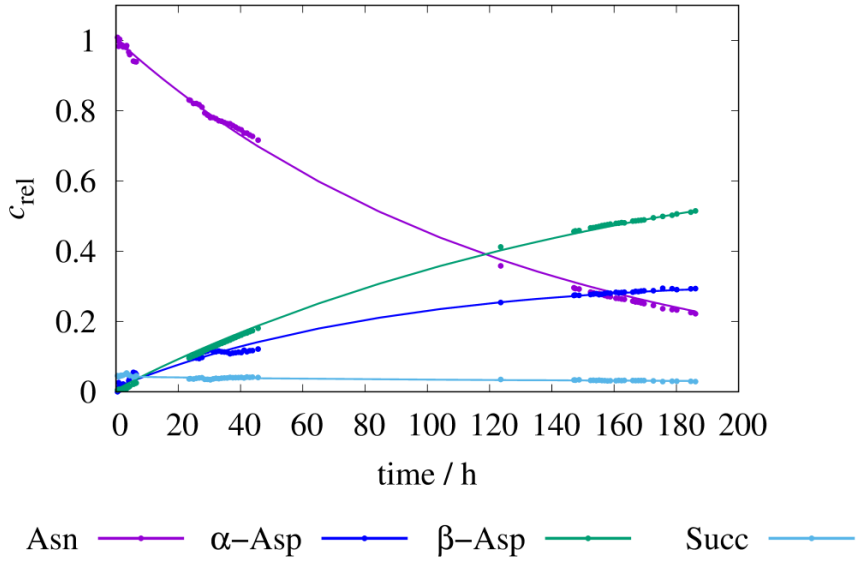

Supplementary Figure 17 **The measured and fitted time course of the Ac-NGRA-NH_2 isomerisation reaction at pH=7.4, 28 °C.** The decomposition of Ac-NGRA-NH_2 via isomerisation and the formation of the products β-Asp (β-DGAA) and α-Asp (α-DGAA), respectively (pH=7.4, T=28 °C), via the intermediate succinimide (Suc). The vertical axis is scaled with arbitrary units proportional to selected non-overlapping NMR signal integrals plotted as a function of the time.

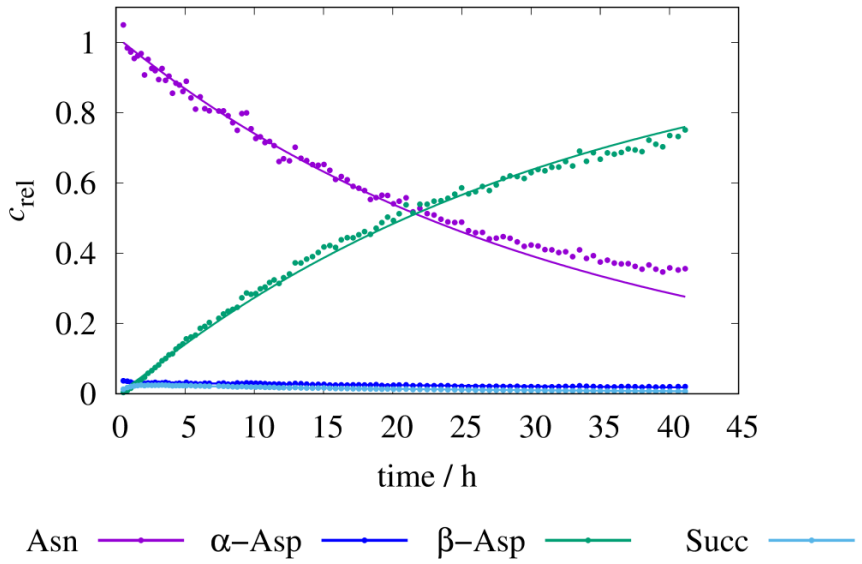

Supplementary Figure 18 **The measured and fitted time course of the Ac-NGRA-NH_2 isomerisation reaction at pH=7.4, 37 °C.** The decomposition of Ac-NGRA-NH_2 via isomerisation and the formation of the products β-Asp (β-DGAA) and α-Asp (α-DGAA), respectively (pH=7.4, T=37 °C), via the intermediate succinimide (Suc). The vertical axis is scaled with arbitrary units proportional to selected non-overlapping NMR signal integrals plotted as a function of the time.

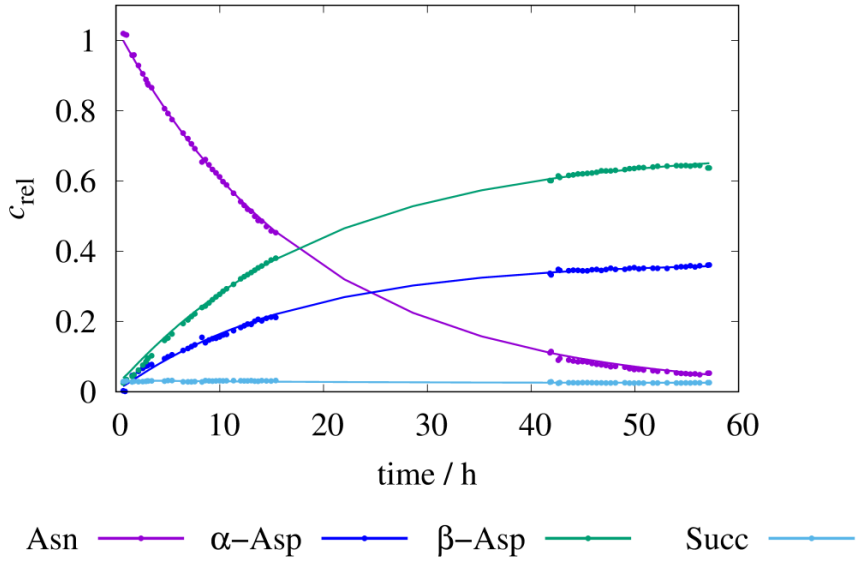

Supplementary Figure 19 **The measured and fitted time course of the Ac-NGRA-NH_2 isomerisation reaction at pH=7.4, 46 °C.** The decomposition of Ac-NGRA-NH_2 via isomerisation and the formation of the products β-Asp (β-DGAA) and α-Asp (α-DGAA), respectively (pH=7.4, T=46 °C), via the intermediate succinimide (Suc). The vertical axis is scaled with arbitrary units proportional to selected non-overlapping NMR signal integrals plotted as a function of the time.

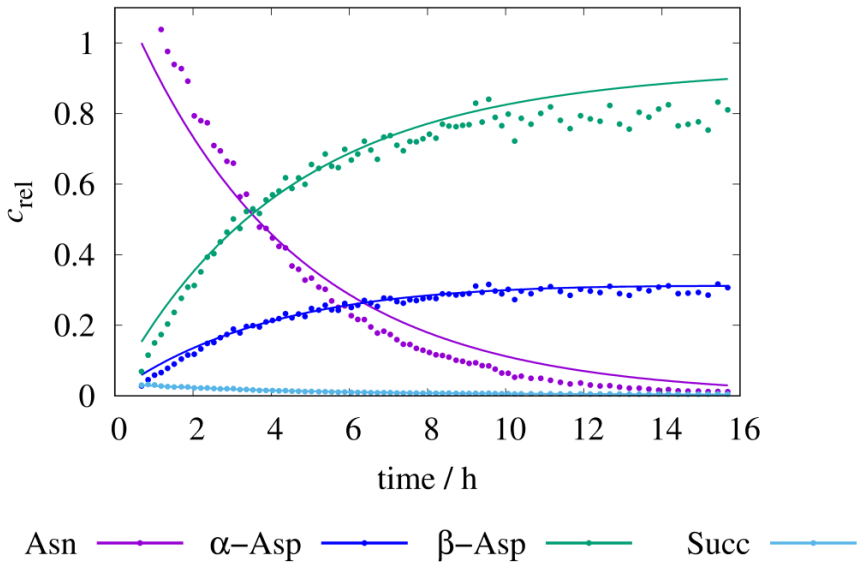

Supplementary Figure 20 **The measured and fitted time course of the Ac-NGRA-NH_2 isomerisation reaction at pH=7.4, 55 °C.** The decomposition of Ac-NGRA-NH_2 via isomerisation and the formation of the products β-Asp (β-DGAA) and α-Asp (α-DGAA), respectively (pH=7.4, T=55 °C), via the intermediate succinimide (Suc). The vertical axis is scaled with arbitrary units proportional to selected non-overlapping NMR signal integrals plotted as a function of the time.

Supplementary Note 3 IRC path calculations and NBO analysis

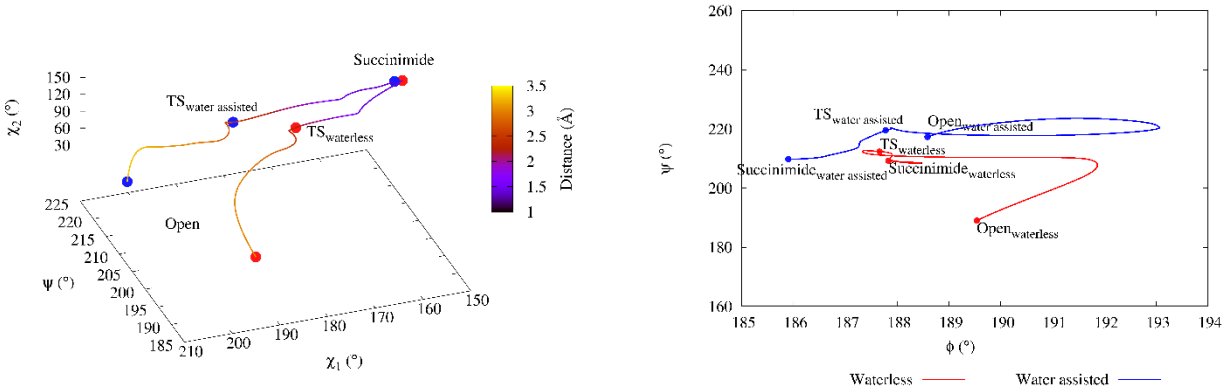

a) **b)**

Supplementary Figure 21 **Variation of asparagine dihedral angles (φ, ψ, χ_1, χ_2) and the Bürgi-Dunitz distance (d) along the calculated IRC pathway**. IRC pathways (B3LYP/6-31+G(d,p) level of theory) from the „open" form of asparagine, towards succinimide formation, for both the waterless (red lines and dots) and the water assisted (blue lines and dots) reactions. The combined change of the side chain dihedral angles creates the spatial arrangement required for the successful reaction. There is no significant change in the peptide backbone (b)), but the χ_1 and χ_2 torsional angles change simultaneously in opposite direction (a)).

The atomic labels in the waterless reaction:

N_{Gly}: the (n+1) amide N-atom of the backbone,
H_{Gly}: the leaving amide proton / the attaching proton to the nitrogen of the asparagine side chain,
N^{δ}_{Asn}: the leaving N-atom of the Asn side chain,
C^{γ}_{Asn}: the carbonyl C-atom of the Asn side chain,
O^{δ}_{Asn}: the carbonyl O-atom of the Asn side chain.

The 4 main step of the waterless reaction along the reaction pathway:
i) During the proton transfer step, the two most significant interacting orbitals are those of LP(1):N^{δ}_{Asn} and σ*(1):N_{Gly}-H_{Gly} with an interaction energy of 535.39 kJ mol^{-1} (Supplementary Figure 23 and Supplementary Table 2). Thus, the N-atom of the Asn side chain donates a lone pair electron to the antibonding orbital σ*(1):N_{Gly}-H_{Gly}, thereby attracting the amide proton from the amide N-atom. *ii)* Thus, the transition state can be formed, in which the major overlapping orbits are LP(1):N_{Gly} with σ*(2):C^{γ}_{Asn}-O^{δ}_{Asn} and LP(2):O^{δ}_{Asn} with σ*(1):C^{γ}_{Asn}-N^{δ}_{Asn} with perturbation energies of 101.92 kJ mol^{-1} and 229.95 kJ mol^{-1}, respectively (Supplementary Figure 24, Supplementary Table 3). This shows that during TS formation, the N_{Gly}-C^{γ}_{Asn} σ-bond formation and breaking of the C^{γ}_{Asn}-N^{δ}_{Asn} σ-bond are simultaneously present. *iii)* The five-membered ring is then closed by the interaction of the LP(3):O^{δ}_{Asn} and the σ*(1):C^{γ}_{Asn}-N^{δ}_{Asn} orbitals and the LP(3):O^{δ}_{Asn} and the σ*(1):N_{Gly}-C^{γ}_{Asn} orbitals, with perturbation energies 242.71 kJ mol^{-1} and 218.41 kJ mol^{-1}, respectively (Supplementary Figure 25 and Supplementary Table 4). In both cases, the electron donor is the side chain O-atom. *iv)* Finally, the reaction reaches the stage where ammonia gas is irreversibly released. The main interaction takes place between the LP(3):O^{δ}_{Asn} and the σ*(1):C^{γ}_{Asn}-N^{δ}_{Asn} orbitals with a perturbation energy of 384.22 kJ mol^{-1}, stabilising the succinimide ring. (Supplementary Figure 26 and Supplementary Table 5).

Tables and figures for the waterless isomerisation reaction:

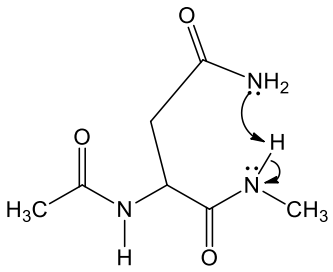

Supplementary Figure 22 **Schematic structure of the open-form of the waterless reaction.**

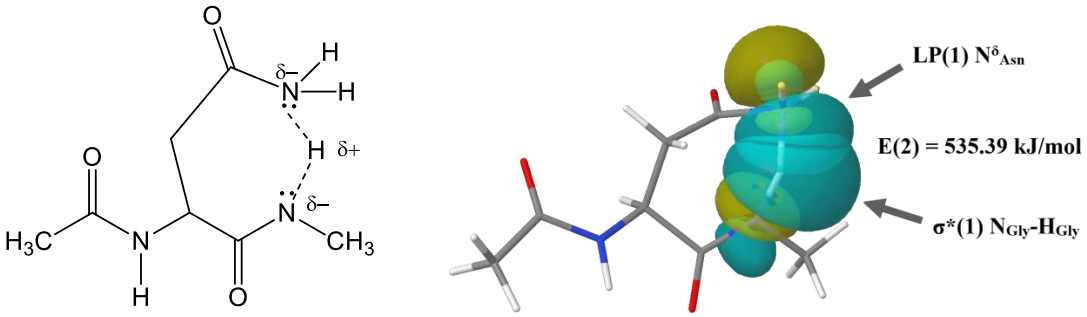

a) b)

Supplementary Figure 23 **Schematic and NBO computational structure of the waterless proton transfer step.** a) Schematic structure of the waterless proton transfer step. b) In the case of the waterless reaction, during the proton transfer step, mainly the LP(1):N^{δ}_{Asn} and the σ*(1):N_{Gly}-H_{Gly} orbitals do overlap.

Supplementary Table 2 Donor-acceptor orbitals and second-order perturbation energies for the proton transfer step of the waterless reaction.

donor	acceptor	$E(2)$ / kJ mol^{-1}
LP(1) N^{δ}_{Asn}	**σ*(1) N_{Gly}-H_{Gly}**	**535.39**
LP(1) N^{δ}_{Asn}	σ*(2) C^{γ}_{Asn}-O^{δ}_{Asn}	26.90
LP(2) O^{δ}_{Asn}	σ*(1) C^{γ}_{Asn}-N^{δ}_{Asn}	181.04

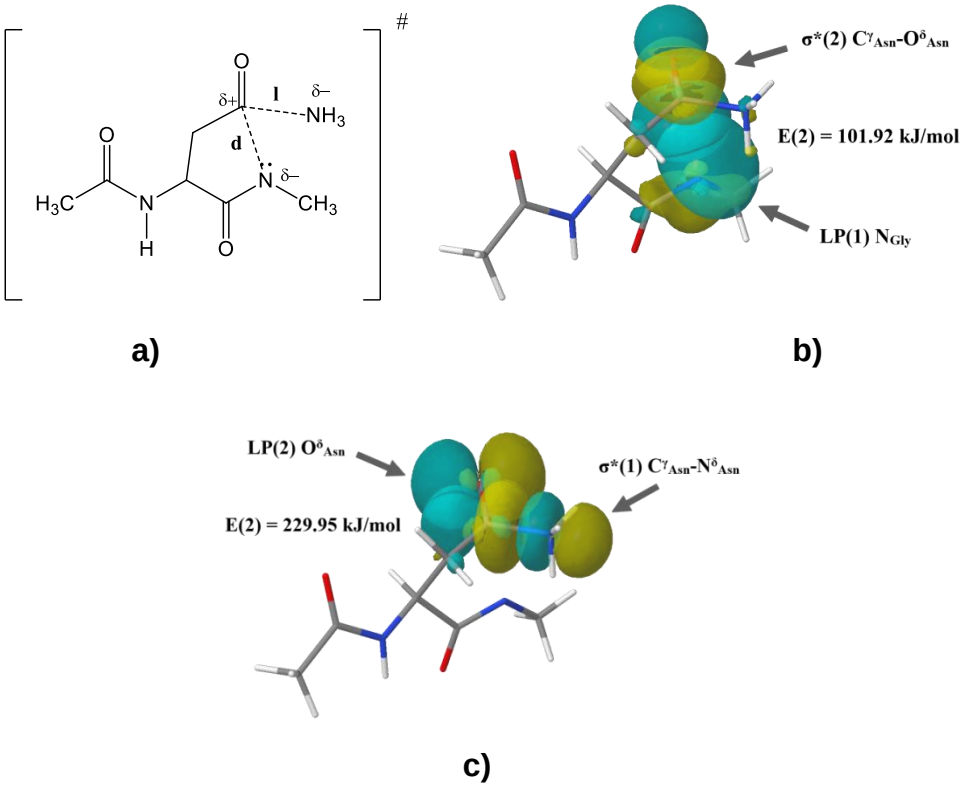

Supplementary Figure 24 **Schematic and NBO computational structure of the waterless transition state.** a) Schematic structure of the waterless transition state. In the case of the waterless reaction, the formation of the N_{Gly}-C' bond, distance d (panel a), and the breaking of the C'-N^{δ}_{Asn} bond, distance l (panel a) are simultaneously present in the TS: b) LP(1):N_{Gly} and σ*(2):C^{γ}_{Asn}-O^{δ}_{Asn} and c) LP(2):O^{δ}_{Asn} and σ*(1):C^{γ}_{Asn}-N^{δ}_{Asn} orbitals overlap.

Supplementary Table 3 Donor-acceptor orbitals and second-order perturbation energies for the TS of the waterless reaction.

donor	acceptor	$E(2)$ / kJ mol^{-1}
LP(1) N_{Gly}	σ*(1) N^{δ}_{Asn}-H_{Gly}	66.61
LP(2) N_{Gly}	σ*(1) N^{δ}_{Asn}-H_{Gly}	10.92
LP(2) O^{δ}_{Asn}	**σ*(1) C^{γ}_{Asn}-N^{δ}_{Asn}**	**229.95**
LP(1) N_{Gly}	**σ*(2) C^{γ}_{Asn}-O^{δ}_{Asn}**	**101.92**
LP(2) N_{Gly}	σ*(2) C^{γ}_{Asn}-O^{δ}_{Asn}	47.11

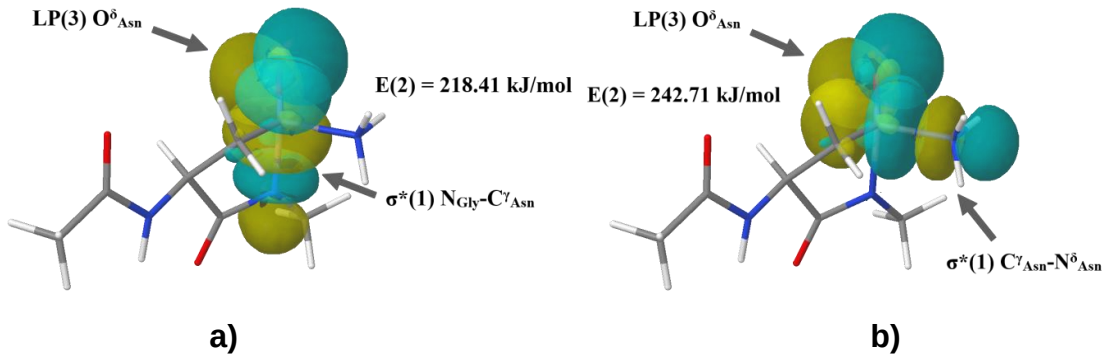

Supplementary Figure 25 **NBO computational structure of the waterless ring closure step.** The key step of the ring closure is when N_{Gly}-C' bond is formed, distance d (Supplementary Figure 24/a), but the C'-N^{δ}_{Asn} bond still remains, distance l (Supplementary Figure 24/a): a) LP(3):O^{δ}_{Asn} and the σ*(1):N_{Gly}-C^{γ}_{Asn} and b) LP(3):O^{δ}_{Asn} and the σ*(1):C^{γ}_{Asn} - N^{δ}_{Asn} orbitals overlap.

Supplementary Table 4 Donor-acceptor orbitals and second-order perturbation energies for the ring closure step of the waterless reaction.

donor	acceptor	E(2) / kJ mol^{-1}
LP(1) N_{Gly}	σ*(1) N^{δ}_{Asn}-H_{Gly}	2.51
LP(3) O^{δ}_{Asn}	**σ*(1) C^{γ}_{Asn}-N^{δ}_{Asn}**	**242.71**
LP(2) O^{δ}_{Asn}	σ*(1) C^{γ}_{Asn}-N^{δ}_{Asn}	124.85
LP(2) O^{δ}_{Asn}	σ*(1) N_{Gly}-C^{γ}_{Asn}	128.03
LP(3) O^{δ}_{Asn}	**σ*(1) N_{Gly}-C^{γ}_{Asn}**	**218.41**

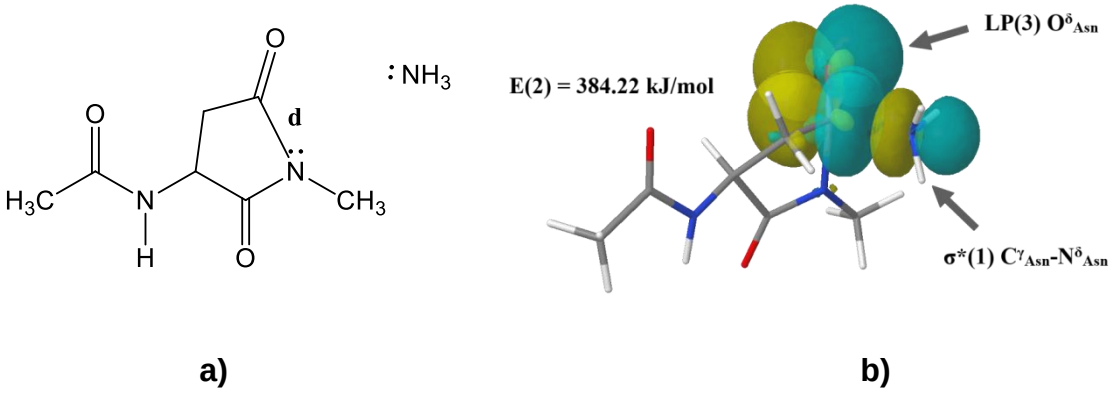

a) **b)**

Supplementary Figure 26 **Schematic and NBO computational structure of the waterless NH_3 release step.** a) Schematic structure of the waterless NH_3 release step. b) During the last step when ammonia gas is release the LP(3):O^{δ}_{Asn} orbital interact with the σ*(1):C^{γ}_{Asn}-N^{δ}_{Asn} orbital.

Supplementary Table 5 Donor-acceptor orbitals and second-order perturbation energies for the ammonia release step of the waterless reaction.

donor	acceptor	E(2) / kJ mol^{-1}
LP(3) O^{δ}_{Asn}	**σ*(1) C^{γ}_{Asn}-N^{δ}_{Asn}**	**384.22**
LP(2) O^{δ}_{Asn}	σ*(1) C^{γ}_{Asn}-N^{δ}_{Asn}	40.92
LP(2) O^{δ}_{Asn}	σ*(1) N_{Gly}-C^{γ}_{Asn}	201.54
LP(3) O^{δ}_{Asn}	σ*(1) N_{Gly}-C^{γ}_{Asn}	94.27

The atomic labels in the water assisted reaction:

N_{Gly}: the (n+1) amide N-atom of the backbone,

H_{Gly}: the leaving amide proton / the attaching proton to the nitrogen of the asparagine side chain,

N^{δ}_{Asn}: the leaving N-atom of the Asn side chain,

C^{γ}_{Asn}: the carbonyl C-atom of the Asn side chain,

O^{δ}_{Asn}: the carbonyl O-atom of the Asn side chain,

O_{H2O}: the O-atom of the explicit water molecule,

H_{H2O}: the leaving proton of the water / the attaching proton to the nitrogen of the asparagine side chain.

Tables for the water assisted isomerisation reaction:

Supplementary Table 6 Donor-acceptor orbitals and second-order perturbation energies during the first proton transfer step of the water assisted reaction.

donor	acceptor	E(2) / kJ mol^{-1}
LP(2) O_{H2O}	σ*(1) N_{Gly}-H_{Gly}	328.99
LP(3) O_{H2O}	σ*(1) N_{Gly}-H_{Gly}	103.89
LP(1) N_{Gly}	σ*(1) N_{Gly}-H_{Gly}	84.56
LP(2) O_{H2O}	σ*(1) N^{δ}_{Asn}-H_{H2O}	2.59
LP(3) O_{H2O}	**σ*(1) N^{δ}_{Asn}-H_{H2O}**	**639.86**
LP(1) O_{H2O}	σ*(1) N^{δ}_{Asn}-H_{H2O}	24.52
LP(2) O^{δ}_{Asn}	σ*(1) C^{γ}_{Asn}-N^{δ}_{Asn}	162.13
LP(1) O^{δ}_{Asn}	σ*(1) C^{γ}_{Asn}-N^{δ}_{Asn}	4.06
LP(1) N_{Gly}	σ*(2) C^{γ}_{Asn}-O^{δ}_{Asn}	19.54

Supplementary Table 7 Donor-acceptor orbitals and second-order perturbation energies during the joint proton transfer step of the water assisted reaction.

donor	acceptor	E(2) / kJ mol^{-1}
LP(2) O_{H2O}	σ*(1) N_{Gly}-H_{Gly}	185.94
LP(3) O_{H2O}	**σ*(1) N_{Gly}-H_{Gly}**	**343.09**
LP(1) N_{Gly}	σ*(1) N_{Gly}-H_{Gly}	96.78
LP(2) O_{H2O}	σ*(1) N^{δ}_{Asn}-H_{H2O}	165.81
LP(3) O_{H2O}	**σ*(1) N^{δ}_{Asn}-H_{H2O}**	**343.38**
LP(1) O_{H2O}	σ*(1) N^{δ}_{Asn}-H_{H2O}	18.41
LP(2) O^{δ}_{Asn}	σ*(1) C^{γ}_{Asn}-N^{δ}_{Asn}	168.95
LP(1) O^{δ}_{Asn}	σ*(1) C^{γ}_{Asn}-N^{δ}_{Asn}	3.89
LP(1) N_{Gly}	σ*(2) C^{γ}_{Asn}-O^{δ}_{Asn}	20.08

Supplementary Table 8 Donor-acceptor orbitals and second-order perturbation energies during the second proton transfer step of the water assisted reaction.

donor	acceptor	E(2) / kJ mol^{-1}
LP(1) N_{Gly}	σ*(1) O_{H2O}-H_{Gly}	306.19
LP(2) N_{Gly}	**σ*(1) O_{H2O}-H_{Gly}**	**379.07**
LP(2) O_{H2O}	σ*(1) O_{H2O}-H_{Gly}	42.47
LP(2) O_{H2O}	σ*(1) N^{δ}_{Asn}-H_{H2O}	343.00
LP(1) O_{H2O}	σ*(1) N^{δ}_{Asn}-H_{H2O}	13.35
LP(2) O^{δ}_{Asn}	σ*(1) C^{γ}_{Asn}-N^{δ}_{Asn}	175.23
LP(1) O^{δ}_{Asn}	σ*(1) C^{γ}_{Asn}-N^{δ}_{Asn}	3.72
LP(1) N_{Gly}	σ*(2) C^{γ}_{Asn}-O^{δ}_{Asn}	26.82
LP(2) N_{Gly}	σ*(2) C^{γ}_{Asn}-O^{δ}_{Asn}	2.51

Supplementary Table 9 Donor-acceptor orbitals and second-order perturbation energies during the TS of the water assisted reaction.

donor	acceptor	E(2) / kJ mol^{-1}
LP(1) N_{Gly}	σ*(1) O_{H2O}-H_{Gly}	137.65
LP(2) N_{Gly}	σ*(1) O_{H2O}-H_{Gly}	97.86
LP(2) O_{H2O}	σ*(1) O_{H2O}-H_{Gly}	3.60
LP(2) O_{H2O}	**σ*(1) N^{δ}_{Asn}-H_{H2O}**	**202.05**
LP(1) O_{H2O}	σ*(1) N^{δ}_{Asn}-H_{H2O}	5.73
LP(2) O^{δ}_{Asn}	**σ*(1) C^{γ}_{Asn}-N^{δ}_{Asn}**	**193.97**
LP(1) O^{δ}_{Asn}	σ*(1) C^{γ}_{Asn}-N^{δ}_{Asn}	3.26
LP(1) N_{Gly}	σ*(2) C^{γ}_{Asn}-O^{δ}_{Asn}	36.86
LP(2) N_{Gly}	σ*(2) C^{γ}_{Asn}-O^{δ}_{Asn}	12.30

Supplementary Table 10 Donor-acceptor orbitals and second-order perturbation energies during the ring closure step of the water assisted reaction.

donor	acceptor	E(2) / kJ mol^{-1}
LP(1) N_{Gly}	σ*(1) O_{H2O}-H_{Gly}	45.02
LP(2) O_{H2O}	σ*(1) N^{δ}_{Asn}-H_{H2O}	82.05
LP(1) O_{H2O}	σ*(1) N^{δ}_{Asn}-H_{H2O}	1.80
LP(1) N_{Gly}	σ*(1) C^{γ}_{Asn}-N_{Gly}	14.64
σ(1) C^{γ}_{Asn}-N^{δ}_{Asn}	σ*(1) C^{γ}_{Asn}-N_{Gly}	5.40
σ(1) C^{γ}_{Asn}-N_{Gly}	σ*(1) C^{γ}_{Asn}-N^{δ}_{Asn}	5.36
LP(1) N_{Gly}	σ*(1) C^{γ}_{Asn}-N^{δ}_{Asn}	9.37
LP(2) O^{δ}_{Asn}	σ*(1) C^{γ}_{Asn}-N^{δ}_{Asn}	180.21
LP(3) O^{δ}_{Asn}	σ*(1) C^{γ}_{Asn}-N^{δ}_{Asn}	100.42
LP(2) O^{δ}_{Asn}	σ*(1) C^{γ}_{Asn}-N_{Gly}	35.61
LP(3) O^{δ}_{Asn}	**σ*(1) C^{γ}_{Asn}-N_{Gly}**	**311.42**
LP(1) N_{Gly}	σ*(1) C^{γ}_{Asn}-O^{δ}_{Asn}	11.38
LP(1) O^{δ}_{Asn}	σ*(1) C^{γ}_{Asn}-N_{Gly}	2.55

Supplementary Table 11 Donor-acceptor orbitals and second-order perturbation energies during the ammonia release step of the water assisted reaction.

donor	acceptor	E(2) / kJ mol^{-1}
LP(1) N_{Gly}	σ*(1) O_{H2O}-H_{Gly}	27.57
LP(2) O_{H2O}	σ*(1) N^{δ}_{Asn}-H_{H2O}	57.57
LP(1) O_{H2O}	σ*(1) N^{δ}_{Asn}-H_{H2O}	1.13
σ(1) C^{γ}_{Asn}-N^{δ}_{Asn}	σ*(1) C^{γ}_{Asn}-N_{Gly}	3.22
σ(1) C^{γ}_{Asn}-N_{Gly}	σ*(1) C^{γ}_{Asn}-N^{δ}_{Asn}	5.23
LP(1) N_{Gly}	σ*(1) C^{γ}_{Asn}-N^{δ}_{Asn}	26.86
LP(2) O^{δ}_{Asn}	σ*(1) C^{γ}_{Asn}-N^{δ}_{Asn}	4.18
LP(3) O^{δ}_{Asn}	**σ*(1) C^{γ}_{Asn}-N^{δ}_{Asn}**	**391.83**
LP(2) O^{δ}_{Asn}	σ*(1) C^{γ}_{Asn}-N_{Gly}	168.87
LP(3) O^{δ}_{Asn}	σ*(1) C^{γ}_{Asn}-N_{Gly}	33.14
LP(1) N_{Gly}	σ*(1) C^{γ}_{Asn}-O^{δ}_{Asn}	22.34
LP(1) O^{δ}_{Asn}	σ*(1) C^{γ}_{Asn}-N_{Gly}	4.14

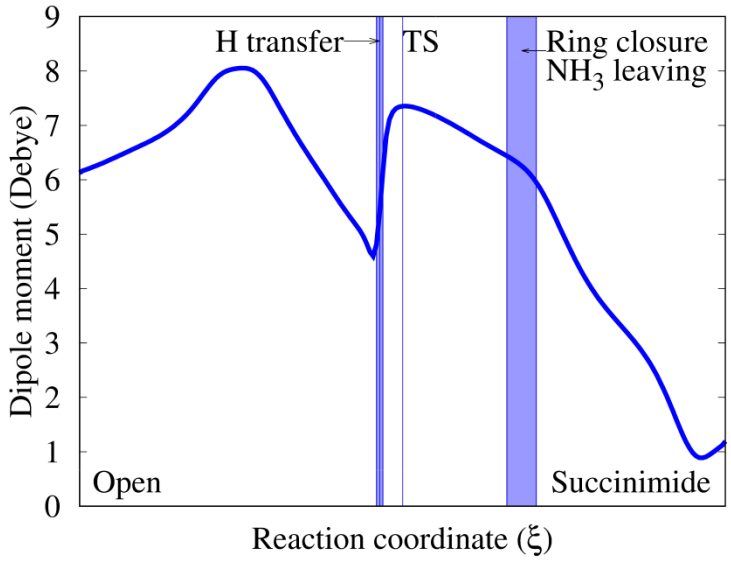

Supplementary Figure 27 **Dipole moment variation along the reaction path, during succinimide formation.** Dipole moment vs. reaction coordinate, ξ, as calculated in vacuum at the B3LYP/6-31+G(d,p) level of theory.

Supplementary Table 12 Selected structural and charge properties of the water assisted oligopeptides: all parameters of the Ac-Asn-Gly-Arg-NH-CH_3 (2) molecule are highly similar, and the key parameters (φ, ψ, χ_1, d(C^{γ}_{Asn}-N_{Gly}), BD angle (N_{Gly}-C^{γ}_{Asn}-O^{δ}_{Asn})) of the Ac-Asn-Gly-Glu-NH-CH_3 (4) molecule are highly different to those of the water assisted transition state (1).

	water assisted TS (1)	water assisted Arg(+) (2)	water assisted Ala (3)	water assisted Glu(-) (4)
φ (°)	-160.17	-162.48	-149.80	-116.03
ψ (°)	-135.64	-146.03	132.14	2.45
χ_1 (°)	177.10	-170.94	-169.25	62.95
χ_2 (°)	-135.25	-135.99	-140.26	-129.02
d(C^{γ}_{Asn}-N_{Gly}) (Å)	2.45	2.77	3.61	3.96
d(N_{Gly}-H_{Gly}) (Å)	1.79	1.76	1.03	1.02
d(O_{H2O}-N_{Gly}) (Å)	2.73	2.74	2.93	6.10
d(O_{H2O}-H_{Gly}) (Å)	1.00	1.00	1.91	6.49
d(O_{H2O}-N^{δ}_{Asn}) (Å)	2.74	2.72	4.79	8.32
d(O_{H2O}-H_{H2O}) (Å)	1.70	1.71	0.98	0.99
d(N^{δ}_{Asn}-H_{H2O}) (Å)	1.06	1.06	3.92	7.69
BD angle (N_{Gly}-C^{γ}_{Asn}-O^{δ}_{Asn}) (°)	108.72	104.43	81.42	62.48
ESP charge C^{γ}_{Asn}	0.66	0.72	0.72	0.72
ESP charge O^{δ}_{Asn}	-0.55	-0.48	-0.63	-0.61
ESP charge N^{δ}_{Asn}	-0.62	-0.68	-0.95	-0.99
ESP charge N_{Gly}	-0.26	-0.48	-0.52	-0.17
ESP charge H_{Gly}	0.33	0.37	0.38	0.22
ESP charge O_{Asn}	-0.75	-0.76	-0.63	-0.64
Δ ESP charge C^{γ}_{Asn} - N_{Gly}[a]	0.91	1.20	1.24	0.88

[a]The reduced Δcharge C^{γ}_{Asn} - N_{Gly} of (2) indicates that the backbone arrangement should also be favorable to enhance isomerisation rate. The calculations were performed at the B3LYP/6-31+G(d) level of theory with the IEFPCM solvent model.